PASJ: Publ. Astron. Soc. Japan **65**, 29, 2013 April 25

VLBI Imagings of a Kilo-Parsec Knot in 3C 380

Shoko KOYAMA,[1,2] Motoki KINO,[3] Hiroshi NAGAI,[2] Kazuhiro HADA,[4] Seiji KAMENO,[5] and Hideyuki KOBAYASHI[1,2]
[1]*Department of Astronomy, Graduate School of Science, The University of Tokyo, 7-3-1 Hongo, Bunkyo-ku, Tokyo 113-0033*
[2]*National Astoronomical Observatory of Japan, 2-21-1 Osawa, Mitaka, Tokyo 181-8588*
shoko.koyama@nao.ac.jp
[3]*The Institute of Space and Astronautical Science, Japan Aerospace Exploration Agency, 3-1-1 Yoshinodai, Chuou-ku, Sagamihara 252-5210*
[4]*INAF Istituto di Radioastronomia, via Gobetti 101, 40129 Bologna, Italy*
[5]*Department of Physics, Faculty of Science, Kagoshima University, 1-21-35 Korimoto, Kagoshima, Kagoshima 890-0065*

(Received 2012 August 22; accepted 2012 October 19)

Abstract

We investigated observational properties of a kilo-parsec scale knot in the radio-loud quasar 3C 380 by using two epoch archival data obtained by Very Long Baseline Interferometry (VLBI) at 5 GHz on 1998 July and 2001 April. We succeed to obtain the highest spatial resolution image of the bright knot K1 located at 732 mas, or $\geqq 20$ kpc deprojected, downstream from the nucleus three-times better than the previously obtained highest-resolution image by Papageorgiou et al. (2006, MNRAS, 373, 449). Our images reveal, with new clarity, an "inverted bow-shock" structure in K1 facing the nucleus; its morphology resembles a conical shock wave. By comparing the two epoch images directly, we explored the kinematics of K1, and obtained the upper limit of the apparent velocity, 0.25 mas yr^{-1} or $9.8c$ of K1 for the first time. The upper limit of the apparent velocity is marginally smaller than superluminal motions seen in the core region. Further new epoch VLBI observations are necessary to measure the proper motion at K1.

Key words: galaxies: active — galaxies: jets — galaxies: quasars: individual (3C 380 = 1828+487) — radio continuum: galaxies — techniques: interferometric

1. Introduction

Thanks to recent progress in the field of radio interferometry, the properties of knots at large scales (down to ~ 100 pc–10 kpc from the nucleus) in several nearby radio galaxies have been investigated. For example, VLBI images clarify the details of complex internal structures, such as knot HST-1 in M 87 ($z = 0.0036$) (e.g., Cheung et al. 2007; Chang et al. 2010; Giroletti et al. 2012), and knot C80 in 3C 120 ($z = 0.033$) (e.g., Roca-Sogorb et al. 2010; Agudo et al. 2012), located 50–100 pc away from their nucleus (details and other examples are summarized in sub-subsection 5.1.1). The HST-1 complex, and knots D and E, located at kpc order from the nucleus of M 87, display superluminal motions of up to $6c$ by Very Large Array (VLA), Hubble space telescope (HST), and VLBI (e.g., Biretta et al. 1995, 1999; Cheung et al. 2007; Chang et al. 2010; Giroletti et al. 2012). The kinematics of knots in the nearby broad-line radio galaxy 3C 120 were also studied out to 3 kpc, but none of the superluminal motion originally claimed by Walker, Walker, and Benson (1988) was found in further VLBI observations (Muxlow & Wilkinson 1991; Walker 1997).

As for radio-loud quasars, VLBI images at large scales, let alone their kinematics, have hardly been studied due to their locations and lack of spatial resolutions. Although the majority of the cores showing superluminal motions are quasars (e.g., Kellermann et al. 2004; Lister et al. 2009), it is not clear where jet deceleration occurs. To develop a detailed understanding of the jet deceleration process and shock dissipation process at large scales, it is crucial to obtain direct images of kpc-scale knots with sufficient spatial resolution. There has been only one attempt to image and constrain on the velocity of kpc-scale knots in radio-loud quasars. With a global VLBI network of 16 radio telescopes, Davis, Unwin, and Muxlow (1991) conducted observations of 3C 273 ($z = 0.158$) at 1.7 GHz. By comparing with an earlier image, they indicated a possible superluminal motion of about $2c$–$5c$ on 100 pc scales, but it is difficult to confirm because different components emerged.

To overcome the above-discribed difficulty and to explore the observational properties of large-scale knots in radio-loud quasars, we selected 3C 380, which is known to be a compact steep spectrum (CSS) radio source ($z = 0.692$) with VLBI. Because of having a steep spectrum, this source is considered to be associated with a misaligned jet (Fanti et al. 1990). Since the position angle of each inner parsec-scale jet, ranging from 284° to 352°, is almost parallel to their motion vectors, it is suggested that the jet was ejected ballistically from the core. There are two distant bright knots, K1 and K2, located $\sim 0\farcs73$ and $1''$ at a position angle around 308°, which is approximately in the direction of the continuation of the inner jet (Kameno et al. 2000). The distance between K1 and the core corresponds to more than 20 kpc, using a viewing angle of $\leqq 15°$ (e.g., Wilkinson et al. 1984; Kameno et al. 2000). The detection of the linear polarization by Multi-Element Radio Linked Interferometer Network (MERLIN) (Flatters 1987) and the optical emission by HST (de Vries et al. 1997) at K1 and K2 implies the presence of strong interactions between the knots and the ambient medium. K1 in 3C 380 is the best target to explore the observational properties of a quasar kpc-scale knot, because the knot is sufficiently bright and the entire angular size of the source is sufficiently compact for VLBI

Table 1. Details of the VLBI observations at 4.815 GHz.

Date	Code	$t_{\rm on}$* (min)	Antennas†	BW‡ (MHz)	Channels§ no.	Channels§ sep. (kHz)	$t_{\rm acc}$‖ (s)
1998/Jul/04	V125	770	VLBA10, EB	16	32	500	4
2001/Apr/24	W410	619	VLBA10	16	128	125	4

* Total on source time.
† Antennas: VLBA10 = Pie town NM USA, Los Alamos NM USA, Fort Davis TX USA, Owens Vally CA USA, Kitt Peak AZ USA, North Liberty IA USA, Hancock NH USA, Brewster WA USA, Saint Croix VI USA, Mauna Kea HI USA. EB: Effelsberg Germany.
‡ Total bandwidth.
§ Channel numbers per 1 IF and channel width per 1 channel.
‖ Data accumulation period.

observations. We attempted to image the kpc-scale knot K1 in 3C 380 with a high-resolution VLBI.

The organization of this paper is as follows. The observation data and data reduction are described in section 2 and section 3, respectively. The results are presented in section 4, and the discussions are given in section 5. Throughout this paper, we adopt the following cosmological parameters: H_0 = 71 km s^{-1} Mpc^{-1}, $\Omega_{\rm M}$ = 0.27, and Ω_Λ = 0.73 (Komatsu et al. 2009), or 1 mas = 7.11 pc and 0.1 mas yr^{-1} = 3.92c.

2. Archival Radio Data

We analyzed two VLBI archival data of the quasar 3C 380 at 4.815 GHz in left-hand circular polarization, observations of which were made on 1998 July 4 and 2001 April 24. In table 1, we summarize the details of the VLBI data. All ten antennas of VLBA (Very Long Baseline Array) were used in the observations. The first epoch is our data as a part of the VSOP (VLBI Space Observatory Programme) observation, including the Effelsberg telescope. The second epoch data were obtained from VLBA archival data services. All of the correlation processes were performed by the National Radio Astronomy Observatory (NRAO) VLBA correlator in Socorro, NM, USA.

3. Data Reduction

We used the Astronomical Image Processing System (AIPS) software package developed by NRAO for a priori amplitude calibration, fringe fitting, and the passband calibration process. For the first epoch data, we did not use the data of spacecraft baselines. Since the distance between the core and K1 corresponds to around 700 beamwidth, time and frequency averaging would cause time and bandwidth smearing in the K1 region (Thompson et al. 2001). To minimize the smearing effect on K1 to make wide field of view images, the frequency channels were averaged within each Intermediate Frequency (IF); these IFs were kept separate during the imaging process. We did not use any time averaging, but the error on each visibility data point was also adopted as the standard deviation within ten seconds by using the AIPS task FIXWT (see table 1).

Imaging was performed using CLEAN and a self-calibration algorithm. This was performed with the Difmap software package (Shepherd et al. 1994). We started imaging the core and the inner jet so as to eliminate the sidelobes from the core over K1, because we expected the K1 flux to be around 10% of the integrated flux density of the inner jets, which was $\sim$2.0 Jy at 5 GHz. We adopted both uniform and natural weighting, and performed phase-only self-calibration several times. After fitting a model to the observed visibility phase, we imaged the inner jet and K1 together by applying natural weighting and uv-tapering, and then performed phase and amplitude self-calibration.

Since all of the data had the shortest uv distance much longer than 143 kλ, which corresponded to half of the beam size of $\sim$720 mas, which covered both the core and K1 at 5 GHz, the missing flux would be caused at K1. Therefore, we only obtained the lower limit of the K1 flux.

4. Results

4.1. Inverted Bow-Shock Structure of K1

In figure 1, we show the overall images of 3C 380 in total intensities. In the left panels, an entire image of 3C 380 and a zoom-in core image are shown, while a K1 image is shown in the right panel with a beam size of 1.66 mas $\times$ 1.10 mas at a beam position angle of $-32\overset{\circ}{.}5$. K1 in figure 1, located at around $0\overset{''}{.}73$ away from the core, was detected with a signal-to-noise ratio (*SNR*) of over eight. From figure 1, we found, with new clarity, an inverted bow-shock shaped structure in the K1 edge-brightened region, as previously described (Simon et al. 1990; Wilkinson et al. 1991; Papageorgiou et al. 2006). This finding helps to confirm the original suggestion of an inverted bow-shock structure in K1 by Cawthorne (2006) and Papageorgiou et al. (2006), with a three-times better resolution than that of their images. The width of K1, measured perpendicular to the jet direction, is about 280 pc (40 mas) which is the same size as the K1 diameter suggested by Simon et al. (1990), and the length of K1 is 140 pc (20 mas), in our images. Compared with the previously obtained VLBI images of K1 (figure 12 in Papageorgiou et al. 2006; top left of figure 1 in Kameno et al. 2000), we attained the highest spatial resolution image by adding the outer five VLBA and the Effelsberg telescopes. The spatial resolution of the obtained K1 image is three-times higher than that of the previously obtained highest resolution image of K1 at 1.6 GHz [the beam size of figure 12

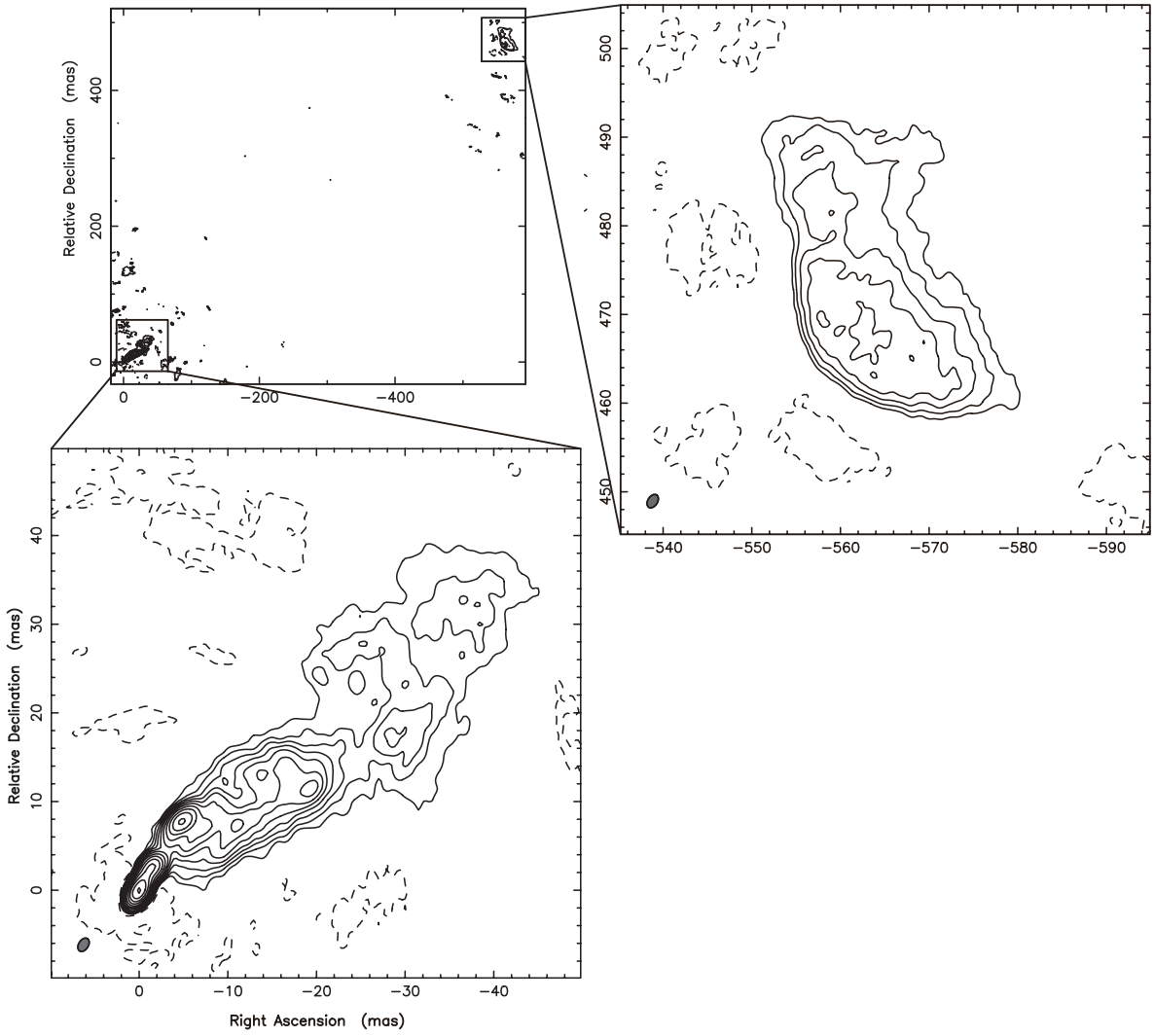

Fig. 1. Top-left panel shows 3C 380 (entire image) obtained by VLBA (ten antennas) plus the Effelsberg telescope on 1998 July 4 at 4.815 GHz with a resolution of 1.66 mas × 1.10 mas in *P.A.* = −32.°5, which is shown at the bottom-left corner of each image. The bottom-left panel displays a zoom-in image around the core with contour levels of 0.328 × (−1, 1, 1.41, 2, 2.83, 4) mJy beam^{-1}. The right panel shows a zoom-in image at K1 with contour levels of 0.328 × (−1, 1, 2, 4, 8, ..., 2056) mJy beam^{-1}. Each lowest contour is at the 3 σ level. Natural weighting was applied.

in Papageorgiou et al. (2006) is 5.0 mas × 3.7 mas].

4.2. Kinematics of K1

We further attempted to explore the kinematics of K1 by comparing Gaussian-fitted peak positions of K1 in our two epoch images. In figure 2, we present the two epoch images of K1, using only the VLBA ten antennas, with the common restored beam size of 2.54 mas × 1.81 mas at a beam position angle of −1.°95 with natural weighting. From figure 2, we find that the inverted bow-shock structure seen in the first epoch image also appears in the second epoch. This structure would have been maintained between these two observations, that is, for over 2.82 yr.

To compare the position of K1 between 1998 July and 2001 April, we overlay two images of figure 2 to produce figure 3 left with a reference to the core peak position measured by the AIPS task JMFIT. Previous studies support that the core brightness peak position converges to a stable point within 0.2 mas order (e.g., O'Sullivan & Gabuzda 2009; Hada et al. 2011). Since it is sufficiently small compared with our beam size, we can regard the core as being stable in the present work. To measure the peak position and to estimate the position accuracy of K1, we fit a single Gaussian model to each slice profile (figure 3 right) by using the task SLFIT in AIPS. From figure 3 right, we find that the core-facing edge of K1 in each epoch is located at the same position, that is, at ∼ 725 mas distance from the core. The full width of half maximum (*FWHM*) of a single Gaussian fitted to a slice profile of K1 is almost

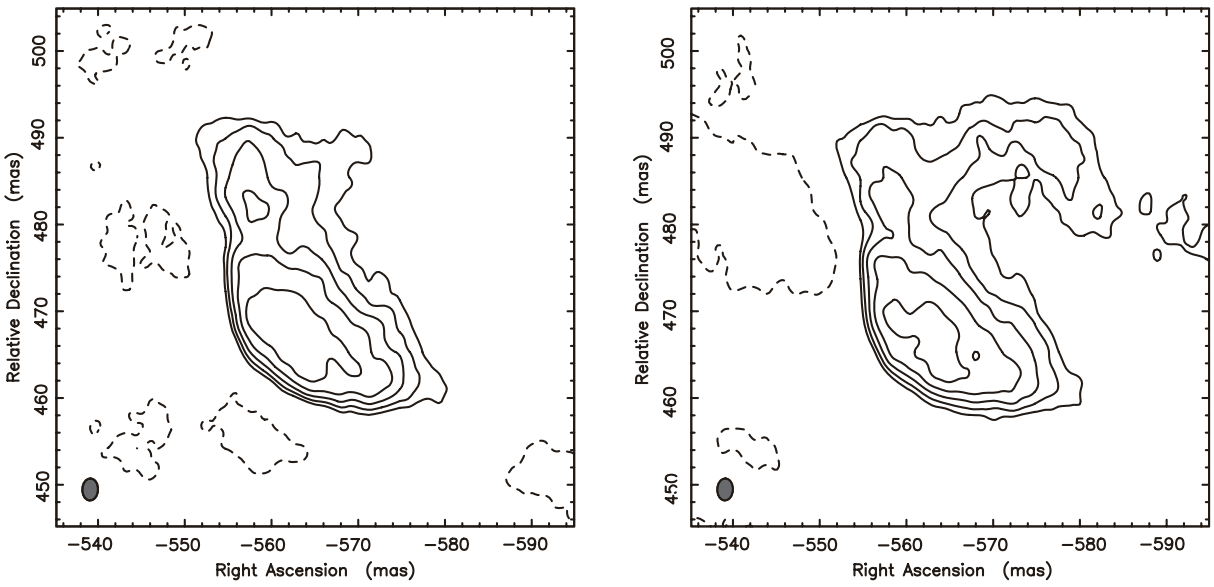

Fig. 2. Natural-weighted images of K1 at 4.815 GHz with VLBA (ten antennas). The left image data was obtained on 1998 July 4, and the right image data was on 2001 April 24. All beam sizes were restored to 2.54 mas × 1.81 mas in *P.A.* = −1.°95, which is the original resolution of the right map. The contour levels are 0.765 × (−1, 1.4142, 2, 2.83, 4) mJy beam^{-1}, which are aligned to the higher 3 σ level (2001 data). Details of these two images are summarized in tables 2 and 3.

Table 2. Image performances of figure 2 with VLBA (ten antennas).

Date	Synthesized beam*			$S_{\rm tot}$ †	$S_{\rm peak}$ ‡	r.m.s.§
	$a_{\rm maj}$ (mas)	$a_{\rm min}$ (mas)	*P.A.* (°)	(Jy)	(mJy beam^{-1})	(mJy beam^{-1})
1998/Jul/04	2.37	1.97	−12.1	2.30	835	0.139
2001/Apr/24	2.54	1.81	−1.95	2.12	934	0.172

* Long axis, short axis, and position angle of synthesized beam.
† Total cleaned flux of the entire image.
‡ Peak flux of the entire image.
§ Root-mean-square noise of the entire map.

identical to a slight change of each image due to the method of self-calibration. The position accuracy of K1 is derived as a ratio of *FWHM* of the fitted Gaussian to *SNR* at K1 (e.g., Walker 1997), which is conservatively estimated to be less than $\sim$0.79 mas. The derived peak positions and their accuracy are summarized in table 3.

Finally, we estimate the maximum apparent velocity of K1, $\beta_{\rm app,max}$, as the peak position displacement over $\Delta t = 2.82$ yr with the propagation of uncertainty. The peak position displacement is $\Delta R = R_1 - R_2 = -0.27$ mas, where R_1 and R_2 are the peak positions at the first epoch and the second epoch, respectively. The error in the displacement is estimated to be 0.97 mas by using the propagation of uncertainty, or the root-mean-square (r.m.s.) of the position uncertainty at each epoch. Therefore, the upper limit of the peak position displacement is $\Delta R_{\rm max} = -0.27 + 0.97 = 0.70$ mas, and the maximum apparent proper motion is estimated to be $\Delta R_{\rm max}/\Delta t = 0.25$ mas yr^{-1}. Thus, we obtain $\beta_{\rm app,max} = 9.8$.

5. Discussion

5.1. Internal Structures in Large-Scale Knots/Hot Spots

5.1.1. Classification of previously known cases

As shown in section 1, VLBI observations of large-scale knots are quite limited, and only a handful of sources have been explored. Here, we classify them. Below, we attempt to categorize the internal structures into three typical ones. We do not include some known sources that are difficult to categorize because of their peculiarities [e.g., HST-1 in M 87 by Giroletti et al. (2012); northern hot spot of the broad line radio galaxy PKS 1421−490 by Godfrey et al. (2009)].

Inverted bow-shock type—As shown in the previous section, the apex of the K1 edge-brightened region in 3C 380 faces towards the core. In this work, we call this feature an inverted bow-shock structure. The same structure as K1 in 3C 380 is found at C80 in 3C 120, which is a stationary jet feature located 140 pc (80 mas) away from the core with 35 pc in size (Agudo et al. 2012). The key common property between 3C 380 and

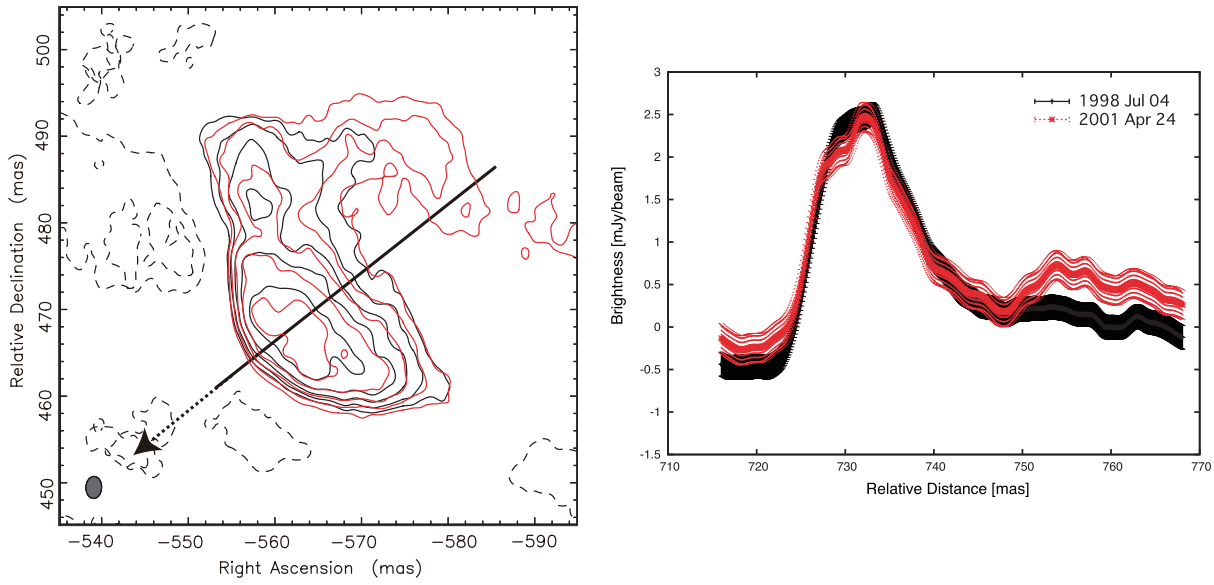

Fig. 3. Left is the 1998 July 4 image overlaid on the 2001 April 24 image shown in figure 2 with reference to the core brightest peak. The straight line shows the slice position. The slice position is determined along the line connecting the core peak position and mean K1 peak position measured by the AIPS task MAXFIT. The dotted arrow indicates the direction to the nucleus. The right image shows slice profiles of K1 along the straight line shown in the left image. We put a 1 σ flux error (or image r.m.s. noise in table 2) on each data point.

Table 3. Properties of K1 in figure 2.

Date	$S_{\rm K1}$* (mJy)	$S_{\rm K1,peak}$† (mJy beam^{-1})	$SNR_{\rm K1}$‡	*FWHM*§ (mas)	Peak position‖ (mas)
1998/Jul/04	$\geqq 152$	$\geqq 2.60$	$\geqq 18.7$	10.42	732.53 ± 0.56
2001/Apr/24	$\geqq 163$	$\geqq 2.41$	$\geqq 14.0$	11.09	732.26 ± 0.79

* Integrated flux of K1 by using the AIPS task IMSTAT.
† Peak flux of K1 derived from the Gaussian model fitted to each slice profile by using the AIPS task SLICE and SLFIT.
‡ *SNR* of K1, or peak flux divided by the r.m.s. noise in table 2. The residual after fitting a Gaussian to each slice profile is as small as the r.m.s. noise of the entire map.
§ *FWHM* of the Gaussian model fitted to the K1 slice profile using SLFIT.
‖ K1 peak position measured by SLFIT. The reference position is the core brightness peak. The position error is *FWHM* over *SNR* of K1.

3C 120 is the viewing angle. They are classified as misaligned AGN (Abdo et al. 2010), since their viewing angles are larger than those of blazars, but smaller than those of radio galaxies.

Bow-shock type—3C 205 is known to be a high-redshift quasar with a large viewing angle, because there exists a pair of strong hot spots. In pioneer work of Lonsdale and Barthel (1998), VLBA images of the primary hot spot A in 3C 205 at 1.4 GHz are shown. The VLBI hot spot, located more than 40 kpc away from the core, has an overall size of 1400 pc, and the jet width is about 250 pc. The apex of the edge-bright region in hot spot A of 3C 205 against the core faces the opposite direction to that of 3C 380. Therefore, we here call this feature a bow-shock type structure to contrast it with the inverted bow-shock type.[1]

Multi-spots type—There are several hot spots having multi-spots in a hot spot. Pictor A is a representative of this. Tingay et al. (2008) revealed that the northwest hot spot in Pictor A at 3.5 kpc scale contains five compact pc-scale components in the spot. The sizes of these components are 30–170 pc. One other example is the southern hot spot of the FRI/FRII radio galaxy PKS 2153−69, which is 200 pc in diameter and contains three components as small as 50 pc (Young et al. 2005). The hot spot is located 5 kpc away from the core, and would trace the varying position of the precessing jet interaction region with clouds.

5.1.2. *Origin of various internal structures*

Bearing the above brief summary in mind, let us discuss possible origins of apparently different internal structures in large-scale knots.

Viewing angle effect—An inverted bow-shock can be observed in broad-line radio galaxies (BLRGs) and CSS-QSOs, both of which have relatively narrow viewing angles. It

[1] Note that Lonsdale and Barthel (1998) focused on the asymmetry of bow-shock, rather than the bow-shock; they discussed a bent-jet model that can explain the asymmetry.

is known that 3C 120 is identified as a BLRG, and its viewing angle is estimated to be $\theta \leqq 19^\circ$ (e.g., Gómez et al. 2000) and CSS-QSO 3C 380 with an inclination angle of $\theta \leqq 15^\circ$ (e.g., Wilkinson et al. 1984; Kameno et al. 2000). On the other hand, the viewing angle of quasar 3C 205 is suggested to be around 40°, which is the upper end of the quasar/radio galaxy unification according to a low lobe flux density ratio (Bridle et al. 1994). Therefore, we speculate that the difference of viewing angles divides images into bow-shock and inverted bow-shock. This point has already been suggested by Cawthorne (2006), by modeling the edge-bright region in K1 as a conical-shock seen with a small viewing angle. Our work contributes to offer the highest resolution image of the K1 structure with new clarity, and to show the inverted bow-shock structure supporting the Cawthorne's model.

Regarding the physical origin of bow-shock and inverted bow-shock, Lind and Blandford (1985) suggested that the bow-shock is caused by a fast stream moving at relativistic speed up the center of the jet while, for example, Norman et al. (1982) indicated that the inverted bow-shock is triggered by a Kelvin–Helmholtz instability inside the unshocked jet. In the case of K1 in 3C 380, the inverted bow-shock might be interpreted as being a bent backflow (reverse shock) at the jet termination point (Mizuta et al. 2010), since Wilkinson et al. (1991) mentioned that K1 is similar to a hot spot seen in the lobes of some Fanaroff–Riley class II sources observed approximately pole-on.

Precession effect—The jet precession effect, or we may also say the jet-jittering effect, was explored and modeled by Scheuer (1982) and Cox, Gull, and Scheuer (1991), and is known as the "dentist drill" model. We consider that when the direction of the straight jet changes, causing the termination point to vary over a large-scale spot larger than the cross section of the jet, dynamically young (or long-lived) relic components can be seen as multi-spots. The multi-spots seen in Pictor A can be explained by dynamically young (or we may say long-lived) relic components produced by the precessing jets (Tingay et al. 2008). They estimated that the typical synchrotron cooling time scale of these regions (from 100 to 700 yr) is much longer than the dynamical (Alfvenic crossing) time scale of a few decades, and indicated that these are dynamically young regions.

5.2. Kinematics of kpc-Scale Knot K1

First of all, we stress that the present work is the first attempt to constrain the upper limit on the possible proper motion at kpc scales in radio-loud quasars. By comparing the Gaussian peak positions of the K1 slice profiles in 1998 July and 2001 April as references to the core peak position (subsection 4.2), we can constrain the resolution of the K1 apparent proper motion up to $0.25\,\mathrm{mas\,yr^{-1}}$, corresponding to an apparent velocity of $\beta_{\mathrm{app,max}} = 9.8$. In the core region, the proper motions of several components were measured by Kameno et al. (2000) and Lister et al. (2009), ranging from $1.2c$ to $15c$, from sub-mas to 30 mas away from the core, respectively. Our constraint is marginally slower than the fastest and outermost apparent motions measured in the core region, which is the apparent motion of component F, $0.38\,\mathrm{mas\,yr^{-1}}$ or $15c$, labeled by Kameno et al. (2000).[2] This implies that jet deceleration or bending occurs between the inner jet and K1, or the ejection angle (viewing angle) of K1 has changed from those of the inner jets, assuming straight ballistic jets. To confirm the jet proper motion at large scales with the maximum resolution of an apparent of velocity of less than $2c$, an additional new epoch VLBI observation having a more than 14-yr interval from the first epoch observation is required. In the case of jet bending, the apparent position angle difference of $\phi_{\mathrm{pos}} \sim 13^\circ$ between F and K1 would be magnified by projection with a fixed small viewing angle ($\theta_{\mathrm{view}} \leqq 15^\circ$). The intrinsic jet bending angle, ϕ_{bend}, is estimated to be $\leqq 3\overset{\circ}{.}3$, where $\tan\phi_{\mathrm{bend}} = \tan\phi_{\mathrm{pos}} \times \sin\theta_{\mathrm{view}}$ (Kameno et al. 2000). As for changes of the jet ejection angle, if we assume the same intrinsic velocity, $\beta = 0.9978$ for F and K1, the viewing angle should be $3\overset{\circ}{.}8$ for component F and $1\overset{\circ}{.}4$ or $10\overset{\circ}{.}2$ for K1.

5.3. Future Prospect

As a first step, we deal with only 5 GHz VLBI data in this paper. Here, we mention future prospects to investigate the properties of K1.

5.3.1. Low-frequency spectrum turnover

Low-frequency spectrum turnover can constrain the jet component properties, such as the magnetic field strength (e.g., PKS 1421−490: Godfrey et al. 2009). Regarding the case of K1 in 3C 380, previous work of Megn et al. (2006) suggested a spectral flattening below ~ 100 MHz. However discussions in Megn et al. (2006) were based on flux values collected from the literature derived from various different interferometers, and in which K1 is smaller than the beam size of each interferometer. Therefore, it seems to be difficult to determine the fluxes accurately. The Square Kilometer Array (SKA)[3] will, in the future, allow us to determine the real turnover frequency with sufficiently high resolution.

5.3.2. Polarization properties

The polarization properties are crucial to explore the magnetic field geometries. Only Papageorgiou et al. (2006) have reported the resolved distribution of the magnetic vector polarization angle (MVPA) in K1. The MVPA distribution appears to be tangential to the inverted bow-shock. In order to clarify a change of the shock structure in K1, the time-variation of MVPA is one of the key quantities for future observations, because a sudden change of MVPA strongly suggests the existence of magnetohydrodynamical fast/slow mode waves (e.g., Nakamura et al. 2011). To clarify the polarization properties of synchrotron emission is also substantial (Nalewajko & Sikora 2012) for testing reconfinement shock models (e.g., Komissarov & Falle 1997; Stawarz et al. 2006; Bromberg & Levinson 2009).

6. Summary

To explore the properties of kpc-scale knots in radio-loud quasars, we produced pc-scale images of a distant knot, K1, in a bright CSS quasar, 3C 380, with VLBI. Below we summarize the main results obtained in this work:

[2] Values are recalculated with the cosmology parameters shown in section 1.
[3] ⟨http://www.skatelescope.org/⟩.

1. Using VLBA plus the Effelsberg telescope at 5 GHz with the technique of wide-field imaging, we succeeded to obtain the highest-resolution images of the pc-scale structure of K1, located at more than 20 kpc downstream from the core. We confirmed the edge-brightened region in K1 on the side facing the core to be inverted bow-shock, which is a clear indication of conical shock with a misaligned viewing angle.
2. Comparing VLBA (ten antennas) images of K1 in 1998 July and 2001 April with reference to the core brightness peak, the edge-brightened regions are located at ~ 725 mas. We constrain the upper limit on the possible proper motion of K1 up to 0.25 mas yr^{-1} or $9.8c$. Since our constraint on the apparent velocity is marginally slower than the fastest knot apparent motions of the core region, jet deceleration, bending, or precession could have occurred. An additional new epoch VLBI observation is needed to confirm the proper motion of K1 with the resolution of the apparent velocity, $\leqq 2c$.

We are grateful to K. Asada and A. Doi for constructive discussions. We thank an anonymous referee for useful comments and suggestions. S.K. acknowledges this research grant provided by the Global COE program of the University of Tokyo. This work was partially supported by a Grant-in-Aid for Scientific Research (KAKENHI 2450240, MK) from Japan Society for the Promotion of Science (JSPS). This research has made use of data from National Radio Astronomy Observatory (NRAO) archive. NRAO is a facility of the National Science Foundation operated under cooperative agreement by Associated Universities, Inc.

References

Abdo, A. A., et al. 2010, ApJ, 720, 912
Agudo, I., Gómez, J. L., Casadio, C., Cawthorne, T. V., & Roca-Sogorb, M. 2012, ApJ, 752, 92
Biretta, J. A., Sparks, W. B., & Macchetto, F. 1999, ApJ, 520, 621
Biretta, J. A., Zhou, F., & Owen, F. N. 1995, ApJ, 447, 582
Bridle, A. H., Hough, D. H., Lonsdale, C. J., Burns, J. O., & Laing, R. A. 1994, AJ, 108, 766
Bromberg, O., & Levinson, A. 2009, ApJ, 699, 1274
Cawthorne, T. V. 2006, MNRAS, 367, 851
Chang, C. S., Ros, E., Kovalev, Y. Y., & Lister, M. L. 2010, A&A, 515, A38
Cheung, C. C., Harris, D. E., & Stawarz, Ł. 2007, ApJ, 663, L65
Cox, C. I., Gull, S. F., & Scheuer, P. A. G. 1991, MNRAS, 252, 558
Davis, R. J., Unwin, S. C., & Muxlow, T. W. B. 1991, Nature, 354, 374
de Vries, W. H., et al. 1997, ApJS, 110, 191
Fanti, R., Fanti, C., Schilizzi, R. T., Spencer, R. E., Rendong, N., Parma, P., van Breugel, W. J. M., & Venturi, T. 1990, A&A, 231, 333
Flatters, C. 1987, Nature, 326, 683
Giroletti, M., et al. 2012, A&A, 538, L10
Godfrey, L. E. H., et al. 2009, ApJ, 695, 707
Gómez, J.-L., Marscher, A. P., Alberdi, A., Jorstad, S. G., & García-Miró, C. 2000, Science, 289, 2317
Hada, K., Doi, A., Kino, M., Nagai, H., Hagiwara, Y., & Kawaguchi, N. 2011, Nature, 477, 185
Kameno, S., Inoue, M., Fujisawa, K., Shen, Z.-Q., & Wajima, K. 2000, PASJ, 52, 1045
Kellermann, K. I., et al. 2004, ApJ, 609, 539
Komatsu, E., et al. 2009, ApJS, 180, 330
Komissarov, S. S., & Falle, S. A. E. G. 1997, MNRAS, 288, 833
Lind, K. R., & Blandford, R. D. 1985, ApJ, 295, 358
Lister, M. L., et al. 2009, AJ, 138, 1874
Lonsdale, C. J., & Barthel, P. D. 1998, AJ, 115, 895
Megn, A. V., et al. 2006, Astron. Rep., 50, 692
Mizuta, A., Kino, M., & Nagakura, H. 2010, ApJ, 709, L83
Muxlow, T. W. B., & Wilkinson, P. N. 1991, MNRAS, 251, 54
Nakamura, M., Meier, D. L., & Garofalo, D. 2011, Ap&SS, 336, 15
Nalewajko, K., & Sikora, M. 2012, A&A, 543, A115
Norman, M. L., Smarr, L., Winkler, K.-H. A., & Smith, M. D. 1982, A&A, 113, 285
O'Sullivan, S. P., & Gabuzda, D. C. 2009, MNRAS, 400, 26
Papageorgiou, A., Cawthorne, T. V., Stirling, A., Gabuzda, D., & Polatidis, A. G. 2006, MNRAS, 373, 449
Roca-Sogorb, M., Gómez, J. L., Agudo, I., Marscher, A. P., & Jorstad, S. G. 2010, ApJ, 712, L160
Scheuer, P. A. G. 1982, in IAU Symp. 97, Extragalactic Radio Sources, ed. D. S. Heeschen & C. M. Wade (Dordrecht: Reidel Publishing Company), 163
Shepherd, M. C., Pearson, T. J., & Taylor, G. B. 1994, Bull. Am. Astron. Soc., 26, 987
Simon, R. S., Readhead, A. C. S., Moffet, A. T., Wilkinson, P. N., Booth, R., Allen, B., & Burke, B. F. 1990, ApJ, 354, 140
Stawarz, Ł., Aharonian, F., Kataoka, J., Ostrowski, M., Siemiginowska, A., & Sikora, M. 2006, MNRAS, 370, 981
Thompson, A. R., Moran, J. M., & Swenson, G. W., Jr. 2001, Interferometry and Synthesis in Radio Astronomy, 2nd ed. (New York: John Wiley & Sons), 119
Tingay, S. J., Lenc, E., Brunetti, G., & Bondi, M. 2008, AJ, 136, 2473
Walker, R. C. 1997, ApJ, 488, 675
Walker, R. C., Walker, M. A., & Benson, J. M. 1988, ApJ, 335, 668
Wilkinson, P. N., Akujor, C. E., Cornwell, T. J., & Saikia, D. J. 1991, MNRAS, 248, 86
Wilkinson, P. N., Booth, R. S., Cornwell, T. J., & Clark, R. R. 1984, Nature, 308, 619
Young, A. J., Wilson, A. S., Tingay, S. J., & Heinz, S. 2005, ApJ, 622, 830